Guided wave characteristics in functionally graded piezoelectric rings with rectangular cross-sections

Jiangong Yu, C. Zhang, Jean-Etienne Lefebvre

J. G. Yu · Ch. Zhang · J. E. Lefebvre

Guided wave characteristics in functionally graded piezoelectric rings with rectangular cross-sections

Abstract For the purpose of design and optimization of functionally graded piezoelectric material (FGPM) transducers, wave propagation in FGPM structures has received much attention in the past twenty years. But previous research efforts have been focused essentially on semi-infinite structures and one-dimensional structures, i.e., structures with a finite dimension in only one direction, such as horizontally infinite flat plates and axially infinite hollow cylinders. This paper proposes a double orthogonal polynomial series approach to solving the wave propagation problem in a two-dimensional FGPM structure, namely an FGPM ring with a rectangular cross-section. By numerical comparison with the available reference results for a purely elastic homogeneous rectangular rod, the validity of the extended polynomial approach is illustrated. The dispersion curves and the electric potential distributions of various FGPM rectangular rings with different material gradient directions, different polarization directions, different radius to thickness ratios, and different width to thickness ratios are calculated to reveal the guided wave characteristics.

1 Introduction

Compared to traditional piezoelectric material transducers, functionally graded piezoelectric material (FGPM) transducers can avoid the incompatibilities that exist between the piezoelectric element and the host structure, i.e., structure under test, such as (i) the residual stress generated during the bonding process, (ii) the interface defects and the possibility of interface crack growth, (iii) severe stress jumps across the interfaces during high electrical actuation or mechanical loading, and (iv) debonding resulted from temperature gradients. The

J. G. Yu (✉)
School of Mechanical and Power Engineering, Henan Polytechnic University,
Jiaozuo 454003, People's Republic of China
E-mail: yu@emails.bjut.edu.cn
Tel.: +8613693919651
Fax: +863913987512

J. G. Yu · Ch. Zhang
Department of Civil Engineering, University of Siegen, 57068 Siegen, Germany

J. E. Lefebvre
Univ Lille Nord de France, 59000 Lille, France

J. E. Lefebvre
UVHC, IEMN-DOAE, 59313 Valenciennes Cedex 9, France

J. E. Lefebvre
CNRS, UMR 8520, 59650 Villeneuve d'Ascq, France

advantages of FGPM have attracted many researchers' attention to develop FGPM transducers by various methods [1–8].

For the purpose of design and optimization of FGPM transducers, many computational models are developed to solve the wave propagation in various FGPM structures in the past thirty years. The most used are various layered models. These models divided an FGM structure into a number of homogeneous or inhomogeneous thin layers, such as finite layer element [9], linearly inhomogeneous layer elements [10], quadratic inhomogeneous layer elements [11], finite elements [12], spectral element [13,14] and versatile transfer matrix approach [15]. There are also some models which took FGM as continuous gradient medium, such as Wentzel–Kramer–Brillouin (WKB) method [16,17], homotopy analysis method [18], and orthogonal polynomial series method [19,20] and analytical solutions for SH waves [21].

So far, previous investigations on wave propagation in FGPM structures have been focused essentially on semi-infinite structures and one-dimensional structures, i.e., structures having a finite dimension in only one direction, such as horizontally infinite flat plates and axially infinite hollow cylinders. But in practical applications, many piezoelectric elements have rather a finite dimension in two directions. Thus, one-dimensional models are not suitable for these structures. This paper presents a double orthogonal polynomial series approach to solving wave propagation problems in a two-dimensional (2-D) FGPM structure, namely an FGPM ring with a rectangular cross-section.

The orthogonal polynomial series approach has been used to solve wave propagation for more than forty years. It has been used to solve wave propagation problems in different structures, from semi-infinite structures [22] to flat plate [19] and to various curved structures [20,23], from purely elastic structures [23] to various multi-field coupled structures [19,24–26], from homogeneous structures [23] to various inhomogeneous structures [22,24–26]. However, the available polynomial series approach can only deal with semi-infinite structures and one-dimensional structures. In such cases, only one orthogonal polynomial series is sufficient to express the displacement in the thickness direction. This paper extends the approach to 2-D structures. A double orthogonal polynomial series is adopted to express the displacements in a rectangular plane, so that the two-dimensional waveguide problems can be solved.

In this paper, two material gradient directions (radial direction and axial direction) and two polarization directions (also radial direction and axial direction) are, respectively, considered. The dispersion curves and the electric potential profiles of various FGPM rectangular rings are presented and discussed. Traction-free and open-circuit boundary conditions are assumed.

2 Governing equations and problem formulation

We consider an orthotropic FGPM ring with a rectangular cross-section, as shown in Fig. 1. In the cylindrical coordinate system (θ, z, r), a, b are the inner and outer radii, d is its thickness in the r direction, and h is its height in the z direction. The radius to thickness ratio is defined as $\eta = b/(b-a)$. Its polarization direction is in the r or z direction.

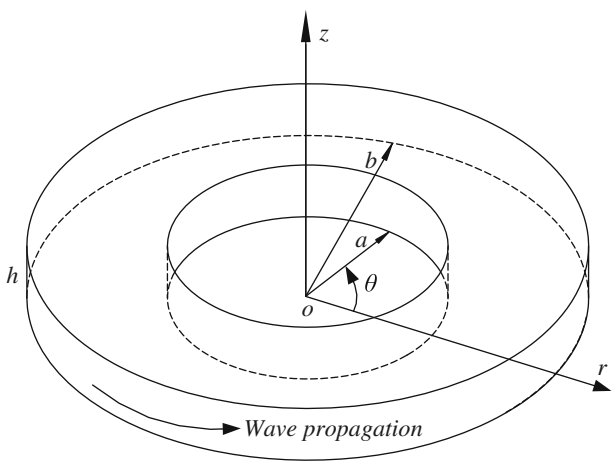

Fig. 1 Schematic diagram of a ring with a rectangular cross-section

For the wave propagation problem considered in this paper, the body forces and electric charges are assumed to be zero. Thus, the dynamic equations of motion for the ring are governed by

$$\begin{aligned}
\frac{\partial T_{rr}}{\partial r}+\frac{1}{r}\frac{\partial T_{r\theta}}{\partial \theta}+\frac{\partial T_{rz}}{\partial z}+\frac{T_{rr}-T_{\theta\theta}}{r}&=\rho\frac{\partial^2 u_r}{\partial t^2},\\
\frac{\partial T_{r\theta}}{\partial r}+\frac{1}{r}\frac{\partial T_{\theta\theta}}{\partial \theta}+\frac{\partial T_{\theta z}}{\partial z}+\frac{2T_{r\theta}}{r}&=\rho\frac{\partial^2 u_\theta}{\partial t^2},\\
\frac{\partial T_{rz}}{\partial r}+\frac{1}{r}\frac{\partial T_{\theta z}}{\partial \theta}+\frac{\partial T_{zz}}{\partial z}+\frac{T_{rz}}{r}&=\rho\frac{\partial^2 u_z}{\partial t^2},\\
\frac{\partial D_r}{\partial r}+\frac{1}{r}\frac{\partial D_\theta}{\partial \theta}+\frac{\partial D_z}{\partial z}+\frac{D_r}{r}&=0
\end{aligned} \tag{1}$$

where T_{ij}, u_i and D_i are the stress, elastic displacement and electric displacement components, respectively, and ρ is the density of the material. In this study, a quasi-electrostatic assumption is made.

The relationships between the strain and displacement components can be expressed as

$$\begin{aligned}
&\varepsilon_{rr}=\frac{\partial u_r}{\partial r},\quad \varepsilon_{\theta\theta}=\frac{1}{r}\frac{\partial u_\theta}{\partial \theta}+\frac{u_r}{r},\quad \varepsilon_{zz}=\frac{\partial u_z}{\partial z},\\
&\varepsilon_{\theta z}=\frac{1}{2}\left(\frac{\partial u_\theta}{\partial z}+\frac{\partial u_z}{r\partial \theta}\right),\quad \varepsilon_{rz}=\frac{1}{2}\left(\frac{\partial u_r}{\partial z}+\frac{\partial u_z}{\partial r}\right),\quad \varepsilon_{r\theta}=\frac{1}{2}\left(\frac{1}{r}\frac{\partial u_r}{\partial \theta}+\frac{\partial u_\theta}{\partial r}-\frac{u_\theta}{r}\right),\\
&E_r=-\frac{\partial \Phi}{\partial r},\quad E_\theta=-\frac{1}{r}\frac{\partial \Phi}{\partial \theta},\quad E_z=-\frac{\partial \Phi}{\partial z}
\end{aligned} \tag{2}$$

where ε_{ij}, E_i and Φ are the strain components, the electric field and the electric potential, respectively.

In this paper, we consider two kinds of FGPM rings, namely the material gradient direction being, respectively, in the radial direction and in the axial direction. For the FGPM ring with a variation of the material properties in the radial direction, we denote it as radially functionally graded piezoelectric or short r-FGPM ring. The elastic parameters of the r-FGPM are dependent on r and can be represented by a polynomial series of the radial coordinate,

$$C_{ij}(r)=C_{ij}^{(0)}+C_{ij}^{(1)}\left(\frac{r}{d}\right)^1+C_{ij}^{(2)}\left(\frac{r}{d}\right)^2+\cdots+C_{ij}^{(L)}\left(\frac{r}{d}\right)^L.$$

With implicit summation over repeated indices, $C_{ij}(r)$ can be written compactly as

$$C_{ij}(r)=C_{ij}^{(l)}\left(\frac{r}{d}\right)^l \quad l=0,1,2,\ldots,L. \tag{3.1}$$

The piezoelectric and dielectric coefficients and the mass density can be treated in the same way, i.e.,

$$e(r)=e_{ij}^{(l)}\left(\frac{r}{d}\right)^l,\quad \in(r)=\in_{ij}^{(l)}\left(\frac{r}{d}\right)^l,\quad \rho(r)=\rho^{(l)}\left(\frac{r}{d}\right)^l,\quad l=0,1,2,\ldots,L. \tag{3.2}$$

The FGPM ring with the material properties varying in the axial direction is referred to as the axially functionally graded piezoelectric or short a-FGPM ring. In this case, the material parameters are functions of z, which can be expressed as

$$C_{ij}(z)=C_{ij}^{(l)}\left(\frac{z}{h}\right)^l, e_{ij}(z)=e_{ij}^{(l)}\left(\frac{z}{h}\right)^l,\quad \in(z)=\in_{ij}^{(l)}\left(\frac{z}{h}\right)^l,\quad \rho(z)=\rho_{ij}^{(l)}\left(\frac{z}{h}\right)^l,\quad l=0,1,2,\ldots,L. \tag{4}$$

Simultaneously, two different polarization directions, i.e., radially polarized and axially polarized directions, will be considered. We use 'rp' and 'ap' to represent these two different polarization directions.

We introduce the function I(r, z)

$$\mathrm{I}(r,z)=\pi(r)\pi(z)=\begin{cases}1, & a\le r\le b \text{ and } 0\le z\le h\\ 0, & \text{elsewhere}\end{cases}$$

where $\pi(r)$ and $\pi(z)$ are rectangular window functions (the subtraction of two Heaviside function) $\pi(r)=\begin{cases}1, & a\le y\le \mathrm{b}\\ 0, & \text{elsewhere}\end{cases}$ and $\pi(z)=\begin{cases}1, & 0\le z\le h\\ 0, & \text{elsewhere}\end{cases}$. The derivatives along r and z of I(r, z) are delta (r)

and delta (z). By introducing the function $\mathrm{I}(r, z)$, the traction-free and open-circuit boundary conditions, i.e., $T_{rr} = T_{r\theta} = T_{rz} = D_r = 0$ at $r = a$, $r = b$ and $T_{rz} = T_{\theta z} = T_{zz}$=$D_z = 0$ at $z = 0$, $z = h$, are automatically incorporated into the constitutive relations of the ring [22]:

$$\begin{aligned}
T_{\theta\theta} &= C_{11}\varepsilon_{\theta\theta} + C_{12}\varepsilon_{zz} + C_{13}\varepsilon_{rr} - e_{31}E_r,\\
T_{zz} &= (C_{12}\varepsilon_{\theta\theta} + C_{22}\varepsilon_{zz} + C_{23}\varepsilon_{rr} - e_{32}E_r)\,\mathrm{I}(r, z),\\
T_{rr} &= (C_{13}\varepsilon_{\theta\theta} + C_{23}\varepsilon_{zz} + C_{33}\varepsilon_{rr} - e_{33}E_r)\mathrm{I}(r, z),\\
T_{rz} &= (2C_{44}\varepsilon_{rz} - e_{24}E_z)\,\mathrm{I}(r, z),\\
T_{r\theta} &= (2C_{55}\varepsilon_{r\theta} - e_{15}E_\theta)\,\mathrm{I}(r, z),\\
T_{\theta z} &= 2C_{66}\varepsilon_{\theta z}\mathrm{I}(r, z),
\end{aligned} \tag{5.1}$$

$$\begin{aligned}
D_\theta &= 2e_{15}\varepsilon_{r\theta} + \in_{11} E_\theta,\\
D_z &= (2e_{24}\varepsilon_{rz} + \in_{22} E_z)\,\mathrm{I}(r, z),\\
D_r &= (e_{31}\varepsilon_{\theta\theta} + e_{32}\varepsilon_{zz} + e_{33}\varepsilon_{rr} + \in_{33} E_r)\,\mathrm{I}(r, z).
\end{aligned} \tag{5.2}$$

In the case of an axial polarization (ap), we have

$$\begin{aligned}
T_{\theta\theta} &= C_{11}\varepsilon_{\theta\theta} + C_{12}\varepsilon_{zz} + C_{13}\varepsilon_{rr} - e_{21}E_z,\\
T_{zz} &= (C_{12}\varepsilon_{\theta\theta} + C_{22}\varepsilon_{zz} + C_{23}\varepsilon_{rr} - e_{22}E_z)\,\mathrm{I}(r, z),\\
T_{rr} &= (C_{13}\varepsilon_{\theta\theta} + C_{23}\varepsilon_{zz} + C_{33}\varepsilon_{rr} - e_{23}E_z)\mathrm{I}(r, z),\\
T_{rz} &= (2C_{44}\varepsilon_{rz} - e_{34}E_r)\,\mathrm{I}(r, z),\\
T_{r\theta} &= 2C_{55}\varepsilon_{r\theta}\mathrm{I}(r, z),\\
T_{\theta z} &= (2C_{66}\varepsilon_{\theta z} - e_{16}E_\theta)\,\mathrm{I}(r, z),
\end{aligned} \tag{6.1}$$

$$\begin{aligned}
D_\theta &= 2e_{16}\varepsilon_{\theta z} + \in_{11} E_\theta,\\
D_z &= (e_{21}\varepsilon_{\theta\theta} + e_{22}\varepsilon_{zz} + e_{23}\varepsilon_{rr} + \in_{22} E_z)\,\mathrm{I}(r, z),\\
D_r &= (2e_{34}\varepsilon_{rz} + \in_{33} E_r)\,\mathrm{I}(r, z)
\end{aligned} \tag{6.2}$$

where C_{ij}, e_{ij} and $\in_{ij}$ are the elastic, piezoelectric and dielectric coefficients given in the crystallographic axes, respectively.

For a free time-harmonic wave propagating in the circumferential direction of a ring, we assume the displacement components to be of the form

$$u_r(r, \theta, z, t) = \exp(ikb\theta - i\omega t)U(r, z), \tag{7.1}$$

$$u_\theta(r, \theta, z, t) = \exp(ikb\theta - i\omega t)V(r, z), \tag{7.2}$$

$$u_z(r, \theta, z, t) = \exp(ikb\theta - i\omega t)W(r, z), \tag{7.3}$$

$$\psi(r, \theta, z, t) = \exp(ikb\theta - i\omega t)X(r, z) \tag{7.4}$$

where $U(r, z)$, $V(r, z)$ and $W(r, z)$ represent the mechanical displacement amplitudes in the r, θ, z directions, respectively, and $X(r, z)$ represents the amplitude of electric potential. Also, k is the magnitude of the wave vector in the propagation direction, and ω is the angular frequency.

Substituting Eqs. (2), (3)/(4), (5)/(6) and (7) into Eq. (1), the governing partial differential equations in terms of the mechanical displacement and electric potential components can be obtained. In the case of the radially polarized (rp) and radially functionally graded piezoelectric (rp-r-FGPM) ring, they are given by

$$\begin{aligned}
&(r/d)^l \left\{ \left[C_{33}^{(l)} \left(r^2 U_{,rr} + (l+1)\, r U_{,r}\right) - \left(C_{11}^{(l)} + (kb)^2 C_{55}^{(l)} - l C_{13}^{(l)}\right) U \right. \right. \\
&+ ikb \left(C_{13}^{(l)} + C_{55}^{(l)}\right) r V_{,r} - ikb \left(C_{11}^{(l)} + C_{55}^{(l)} - l C_{13}^{(l)}\right) V + \left(C_{23}^{(l)} + C_{44}^{(l)}\right) r^2 W_{,rz} \\
&+ \left((l+1)\, C_{23}^{(l)} - C_{12}^{(l)}\right) r W_{,z} + C_{44}^{(l)} r^2 U_{,zz} + e_{33}^{(l)} \left(r^2 X_{,rr} + (l+1)\, r X_{,r}\right) \\
&\left. - e_{31}^{(l)} r X_{,r} - (kb)^2 e_{15}^{(l)} X + e_{24}^{(l)} r^2 X_{,zz} \right] I(r, z) \\
&+ \left[C_{33}^{(l)} r^2 U_{,r} + C_{13}^{(l)} r\, (ikbV + U) + C_{23}^{(l)} r^2 W_{,z} + e_{33}^{(l)} r^2 X_{,r} \right] I(r, z)_{,r} \\
&\left. + \left[C_{44}^{(l)} r^2 \left(U_{,z} + W_{,r}\right) + e_{24}^{(l)} r^2 X_{,z} \right] I(r, z)_{,z} \right\} = -(r/d)^l \rho^{(l)} r^2 \omega^2 U,
\end{aligned} \tag{8.1}$$

$$(r/d)^l \left\{\left[C_{55}^{(l)}\left(r^2V_{,rr}+(l+1)\,rV_{,r}\right)-\left((l+1)\,C_{55}^{(l)}+(kb)^2\,C_{11}^{(l)}\right)V+ikb\left(C_{13}^{(l)}+C_{55}^{(l)}\right)rU_{,r}\right.\right.$$
$$+C_{66}^{(l)}r^2V_{,zz}+ikb\left(C_{11}^{(l)}+(l+1)\,C_{66}^{(l)}\right)U+ikb\left(C_{12}^{(l)}+C_{66}^{(l)}\right)rW_{,z}+\left(e_{31}^{(l)}+e_{15}^{(l)}\right)rX_{,r}$$
$$\left.+2e_{15}^{(l)}X+\right]I(r,z)+C_{66}^{(l)}\left(r^2V_{,z}+ikbrW\right)I(r,z)_{,z}$$
$$\left.+\left[C_{55}^{(l)}\left(r^2V_{,r}+rV+ikbrU\right)+e_{15}^{(l)}rX\right]I(r,z)_{,r}\right\}=-(r/d)^l\,\rho^{(l)}r^2\omega^2V, \tag{8.2}$$

$$(r/d)^l \left\{\left[C_{44}^{(l)}\left(r^2W_{,rr}+(l+1)\,rW_{,r}\right)-(kb)^2\,C_{66}^{(l)}W+C_{22}^{(l)}r^2W_{,zz}+\left(C_{23}^{(l)}+C_{44}^{(l)}\right)r^2U_{,rz}\right.\right.$$
$$+\left(C_{12}^{(l)}+(l+1)\,C_{44}^{(l)}\right)rU_{,z}+ikb\left(C_{12}^{(l)}+C_{66}^{(l)}\right)rV_{,z}+\left(e_{24}^{(l)}+e_{32}^{(l)}\right)r^2X_{,rz}+(l+1)\,e_{24}^{(l)}rX_{,z}\left.\right]I(r,z)$$
$$+\left[C_{23}^{(l)}r^2U_{,r}+C_{12}^{(l)}r\,(ikbV+U)+C_{22}^{(l)}r^2W_{,z}+e_{32}^{(l)}r^2X_{,r}\right]I(r,z)_{,z}$$
$$\left.+\left[C_{44}^{(l)}r^2\,(W_{,r}+U_{,z})+e_{24}^{(l)}r^2X_{,z}\right]I(r,z)_{,r}\right\}=-(r/d)^l\,\rho^{(l)}r^2\omega^2V, \tag{8.3}$$

$$(r/d)^l \left\{\left[e_{33}^{(l)}\left(r^2U_{,rr}+(l+1)\,rU_{,r}\right)+e_{31}^{(l)}rU_{,r}-(kb)^2\,e_{15}^{(l)}U+le_{31}^{(l)}U+e_{24}^{(l)}r^2U_{,zz}+le_{31}^{(l)}V\right.\right.$$
$$-e_{15}^{(l)}V+\left(e_{31}^{(l)}+e_{15}^{(l)}\right)rV_{,r}+\left(e_{24}^{(l)}+e_{32}^{(l)}\right)r^2W_{,rz}+\left(e_{24}^{(l)}+le_{32}^{(l)}\right)rW_{,z}+(kb)^2\in_{11}^{(l)}X$$
$$\left.-\in_{33}^{(l)}\left(r^2X_{,rr}+(l+1)\,rX_{,r}\right)-\in_{22}^{(l)}r^2X_{,zz}\right]I(r,z).$$
$$+\left[e_{24}^{(l)}r^2U_{,z}+e_{24}^{(l)}r^2W_{,r}-\in_{22}^{(l)}r^2X_{,z}\right]I(r,z)_{,z}$$
$$\left.+\left[e_{33}^{(l)}r^2U_{,r}+e_{31}^{(l)}rU+e_{31}^{(l)}rV+e_{32}^{(l)}r^2W_{,z}-\in_{33}^{(l)}r^2X_{,r}\right]I(r,z)_{,r}\right\}=0 \tag{8.4}$$

where a subscript comma indicates partial derivative with respect to spatial coordinates.

To solve the coupled wave equations, $U(r,z)$, $V(r,z)$, $W(r,z)$ and $X(r,z)$ are expanded into products of two Legendre orthogonal polynomial series as

$$\begin{aligned} U(r,z)&=\sum_{m,j=0}^{\infty}p_{m,j}^1\,Q_m(r)\,Q_j(z), \quad V(r,z)=\sum_{m,j=0}^{\infty}p_{m,j}^2\,Q_m(r)\,Q_j(z),\\ W(r,z)&=\sum_{m,j=0}^{\infty}p_{m,j}^3\,Q_m(r)\,Q_j(z), \quad X(r,z)=\sum_{m,j=0}^{\infty}p_{m,j}^4\,Q_m(r)\,Q_j(z)\end{aligned} \tag{9}$$

where $p_{m,j}^i(i=1,2,3,4)$ is the expansion coefficients and

$$Q_m(r)=\sqrt{\frac{2m+1}{b-a}}P_m\left(\frac{2r-b-a}{b-a}\right), \quad Q_j(z)=\sqrt{\frac{2j+1}{h}}P_j\left(\frac{2z-h}{h}\right), \tag{10}$$

with P_m and P_j being the mth and the jth Legendre polynomials. Theoretically, m and j run from 0 to ∞. However, in practice, the summation over the polynomials in Eq. (9) can be truncated at some finite values $m=M$ and $j=J$, when the effects of higher order terms become negligible.

Equation (8) is multiplied by $Q_{\rm n}(r)$ with n running from 0 to M, and by $Q_p(z)$ with p from 0 to J, respectively. Then, integrating over z from 0 to h and over r from a to b gives the following system of linear algebraic equations:

$${}^lA_{11}^{n,p,m,j}p_{m,j}^1+{}^lA_{12}^{n,p,m,j}p_{m,j}^2+{}^lA_{13}^{n,p,m,j}p_{m,j}^3+{}^lA_{14}^{n,p,m,j}p_{m,j}^4=-\omega^2\cdot{}^lM_{n,p,m,j}p_{m,j}^1, \tag{11.1}$$
$${}^lA_{21}^{n,p,m,j}p_{m,j}^1+{}^lA_{22}^{n,p,m,j}p_{m,j}^2+{}^lA_{23}^{n,p,m,j}p_{m,j}^3+{}^lA_{24}^{n,p,m,j}p_{m,j}^4=-\omega^2\cdot{}^lM_{n,p,m,j}p_{m,j}^2, \tag{11.2}$$
$${}^lA_{31}^{n,p,m,j}p_{m,j}^1+{}^lA_{32}^{n,p,m,j}p_{m,j}^2+{}^lA_{33}^{n,p,m,j}p_{m,j}^3+{}^lA_{34}^{n,p,m,j}p_{m,j}^4=-\omega^2\cdot{}^lM_{n,p,m,j}p_{m,j}^3, \tag{11.3}$$
$${}^lA_{41}^{n,p,m,j}p_{m,j}^1+{}^lA_{42}^{n,p,m,j}p_{m,j}^2+{}^lA_{43}^{n,p,m,j}p_{m,j}^3+{}^lA_{44}^{n,p,m,j}p_{m,j}^4=0 \tag{11.4}$$

where ${}^lA_{\alpha\beta}^{n,p,m,j}(\alpha,\beta=1,2,3,4)$ and ${}^lM_{n,p,m,j}$ are the elements of the non-symmetric matrices A and M, which can be obtained by using Eq. (8).

Equation (11.4) can be written as

$$p_{m,j}^{4} = -\left({}^{l}A_{44}^{n,p,m,j}\right)^{-1}\left({}^{l}A_{41}^{n,p,m,j}\,p_{m,j}^{1} + {}^{l}A_{42}^{n,p,m,j}\,p_{m,j}^{2} + {}^{l}A_{43}^{n,p,m,j}\,p_{m,j}^{3}\right). \tag{12}$$

Substituting Eq. (12) into Eqs. (11.1)–(11.3) gives

$$\begin{aligned}
&\left[{}^{l}A_{11}^{n,p,m,j} - {}^{l}A_{14}^{n,p,m,j}\left({}^{l}A_{44}^{n,p,m,j}\right)^{-1}\cdot{}^{l}A_{41}^{n,p,m,j}\right]p_{m,j}^{1}\\
&\quad+\left[{}^{l}A_{12}^{n,p,m,j} - {}^{l}A_{14}^{n,p,m,j}\left({}^{l}A_{44}^{n,p,m,j}\right)^{-1}\cdot{}^{l}A_{42}^{n,p,m,j}\right]p_{m,j}^{2}\\
&\quad+\left[{}^{l}A_{13}^{n,p,m,j} - {}^{l}A_{14}^{n,p,m,j}\left({}^{l}A_{44}^{n,p,m,j}\right)^{-1}\cdot{}^{l}A_{43}^{n,p,m,j}\right]p_{m,j}^{3} = -\omega^{2l}M_{n,p,m,j}\,p_{m,j}^{1}, \qquad (13.1)\\
&\left[{}^{l}A_{21}^{n,p,m,j} - {}^{l}A_{24}^{n,p,m,j}\left({}^{l}A_{44}^{n,p,m,j}\right)^{-1}\cdot{}^{l}A_{41}^{n,p,m,j}\right]p_{m,j}^{1}\\
&\quad+\left[{}^{l}A_{22}^{n,p,m,j} - {}^{l}A_{24}^{n,p,m,j}\left({}^{l}A_{44}^{n,p,m,j}\right)^{-1}\cdot{}^{l}A_{42}^{n,p,m,j}\right]p_{m,j}^{2}\\
&\quad+\left[{}^{l}A_{23}^{n,p,m,j} - {}^{l}A_{24}^{n,p,m,j}\left({}^{l}A_{44}^{n,p,m,j}\right)^{-1}\cdot{}^{l}A_{43}^{n,p,m,j}\right]p_{m,j}^{3} = -\omega^{2l}M_{n,p,m,j}\,p_{m,j}^{2}, \qquad (13.2)\\
&\left[{}^{l}A_{31}^{n,p,m,j} - {}^{l}A_{34}^{n,p,m,j}\left({}^{l}A_{44}^{n,p,m,j}\right)^{-1}\cdot{}^{l}A_{41}^{n,p,m,j}\right]p_{m,j}^{1}\\
&\quad+\left[{}^{l}A_{32}^{n,p,m,j} - {}^{l}A_{34}^{n,p,m,j}\left({}^{l}A_{44}^{n,p,m,j}\right)^{-1}\cdot{}^{l}A_{42}^{n,p,m,j}\right]p_{m,j}^{2}\\
&\quad+\left[{}^{l}A_{33}^{n,p,m,j} - {}^{l}A_{34}^{n,p,m,j}\left({}^{l}A_{44}^{n,p,m,j}\right)^{-1}\cdot{}^{l}A_{43}^{n,p,m,j}\right]p_{m,j}^{3} = -\omega^{2l}M_{n,p,m,j}\,p_{m,j}^{3}. \qquad (13.3)
\end{aligned}$$

Then, Eq. (11) can be rewritten as

$$\begin{bmatrix}
{}^{l}\bar{A}_{11}^{n,p,m,j} & {}^{l}\bar{A}_{12}^{n,p,m,j} & {}^{l}\bar{A}_{13}^{n,p,m,j}\\
{}^{l}\bar{A}_{21}^{n,p,m,j} & {}^{l}\bar{A}_{22}^{n,p,m,j} & {}^{l}\bar{A}_{22}^{n,p,m,j}\\
{}^{l}\bar{A}_{31}^{n,p,m,j} & {}^{l}\bar{A}_{32}^{n,p,m,j} & {}^{l}\bar{A}_{33}^{n,p,m,j}
\end{bmatrix}\begin{Bmatrix} p_{m,j}^{1}\\ p_{m,j}^{2}\\ p_{m,j}^{3}\end{Bmatrix} = -\omega^{2l}M_{n,p,m,j}\begin{bmatrix}1&0&0\\0&1&0\\0&0&1\end{bmatrix}\begin{Bmatrix} p_{m,j}^{1}\\ p_{m,j}^{2}\\ p_{m,j}^{3}\end{Bmatrix}. \tag{14}$$

So, Eq. (14) forms the eigenvalue problem to be solved. The eigenvalues ω^2 give the angular frequency of the guided wave modes, and the eigenvectors $p_{m,j}^{i}$ ($i = 1, 2, 3$) allow the mechanical displacement components to be calculated, and $p_{m,j}^{4}$, which can be obtained from Eq. (12), determines the electric potential distribution. By using the relation $Vph = \omega/k$, the phase wave velocity Vph can be obtained. In the computing progress, the obtained eigenvalues are complex, but their imaginary parts are all very small compared to their corresponding real parts. For one eigenvalue, its imaginary part is less than one millionth of its real part. So, we just think the real parts are solutions of the system.

3 Numerical results

The Voigt-type model is used in this study to calculate the effective parameters of the FGM ring, which can be expressed as

$$C(r) = C_1V_1(r) + C_2V_2(r) \quad \text{for r-FGPM rectangular ring,} \tag{15.1}$$

$$C(z) = C_1V_1(z) + C_2V_2(z) \quad \text{for a-FGPM rectangular ring} \tag{15.2}$$

where $V_i(r/z)$ and C_i denote the volume fraction of the ith material and the corresponding property of the ith material, respectively, and $\sum V_i(r) = \sum V_i(z) = 1$. So, the properties of the FGM can be expressed as

$$C(r) = C_2 + (C_1 - C_2)\, V_1(r) \quad \text{for r-FGPM rectangular ring,} \tag{16.1}$$
$$C(z) = C_2 + (C_1 - C_2)\, V_1(z) \quad \text{for a-FGPM rectangular ring.} \tag{16.2}$$

According to Eqs. (3) and (4), the gradient profile of the material volume fraction can be expressed as a power series expansion. The coefficients of the power series can be determined using the Mathematica function 'Fit'.

Based on the mathematical formulation as presented in Sect. 2, computer programs in terms of the extended polynomial method have been written using Mathematica to calculate the dispersion curves as well as the mechanical displacement and the electrical potential distributions for the FGM rectangular rings.

3.1 Comparison with the reference solution

So far, no reference results for the guided waves in rings with a rectangular cross-section can be found in the literature, we consider a homogeneous steel ring of a square cross-section with a very large radius to thickness ratio $\eta = 1{,}000$ to make a comparison with known results of a straight steel square bar from the semi-analytical finite element method [27]. For the square steel bar, $C_{\mathrm{L}} = 5.85$ km/s, $C_{\mathrm{T}} = 3.23$ km/s and $h = d = 5.08$ mm. Here, C_{L} and C_{T} are, respectively, the longitudinal and the transverse wave velocities. Figure 2 shows the corresponding dispersion curves, where dotted lines are from Hayashi et al. [27] and solid lines are obtained from the present polynomial approach. As can be seen, the results from the extended polynomial approach agree well with the reference data, which verifies the correctness and the accuracy of the present method.

3.2 Dispersion curves for FGPM rectangular rings

The FGPM rings are composed of PZT-4 (bottom surface for a-FGPM rectangular ring and inner surface for r-FGPM rectangular ring) and BSN. The corresponding material parameters are given in Table 1. Here, the

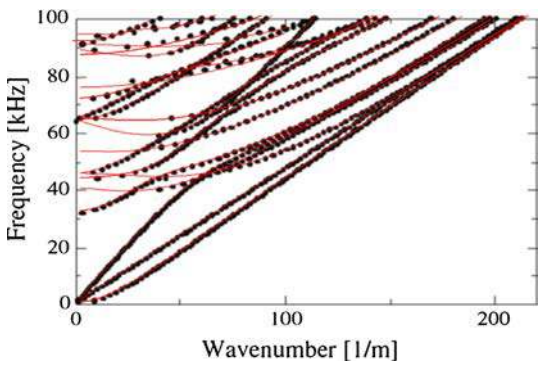

Fig. 2 Dispersion curves for the steel structures with square cross-sections (*dotted lines* the results from the semi-analytical FEM [27] for the straightly steel rod, *solid lines* the results of the presented method for the steel ring with a very large radius to thickness ratio ($\eta = 1{,}000$))

Table 1 Physical parameters of the two piezoelectric materials

Property	C_{11}	C_{12}	C_{13}	C_{22}	C_{23}	C_{33}	C_{44}	C_{55}	C_{66}
PZT-4	13.9	7.4	7.4	13.9	7.4	11.5	2.56	2.56	3.05
BSN	23.9	10.4	5	24.7	5.2	13.5	6.5	6.6	7.6
r-polarization	e_{15}	e_{24}	e_{31}	e_{32}	e_{33}	ε_{11}	ε_{22}	ε_{33}	ρ
PZT-4	12.7	12.7	−5.2	−5.2	15.1	650	650	560	7.5
BSN	2.8	3.4	−0.4	−0.3	4.3	196	201	28	5.3
a-polarization	e_{34}	e_{16}	e_{23}	e_{21}	e_{22}	ε_{33}	ε_{11}	ε_{22}	ρ
PZT-4	12.7	12.7	−5.2	−5.2	15.1	650	650	560	7.5
BSN	2.8	3.4	−0.4	−0.3	4.3	196	201	28	5.3

Units: C_{ij} (10^{10} N/m^2), ε_{ij} (10^{-11} F/m), e_{ij} (C/m^2), ρ (10^3kg/m^3)

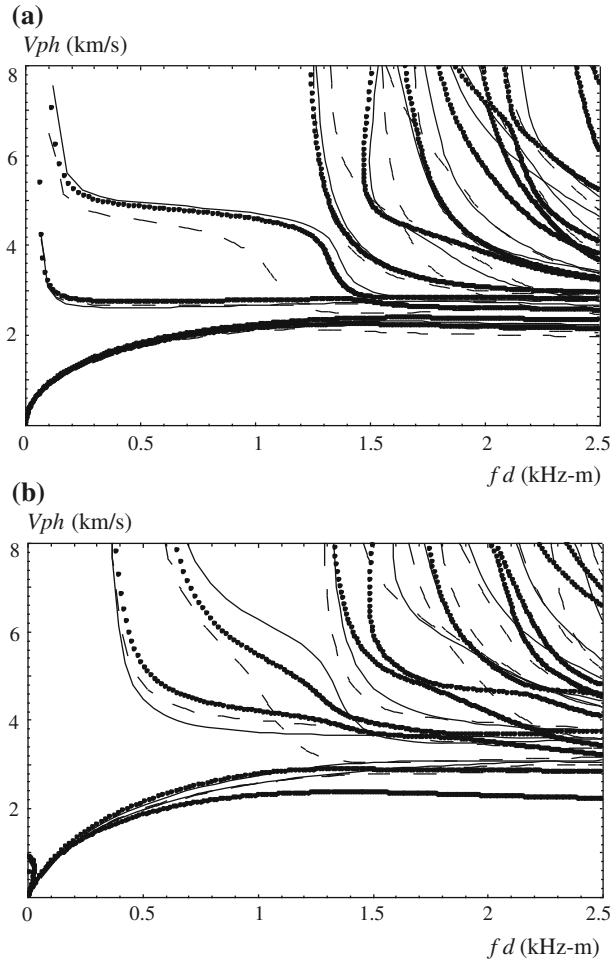

Fig. 3 Phase velocity dispersion curves for linearly FGPM square rings (*solid lines* r-polarized r-FGPM ring, *dashed lines* a-polarized r-FGPM ring, *dotted lines* r-polarized a-FGPM ring): **a** with $\eta = 10$, **b** with $\eta = 2$

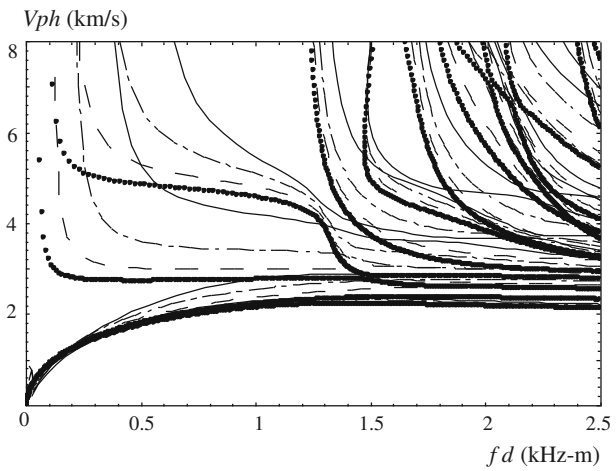

Fig. 4 Phase velocity dispersion curves for r-polarized and linearly a-FGPM square rings (*solid lines* $\eta = 10$, *long-short lines* $\eta = 5$, *dashed lines* $\eta = 3$, *dotted lines* $\eta = 2$)

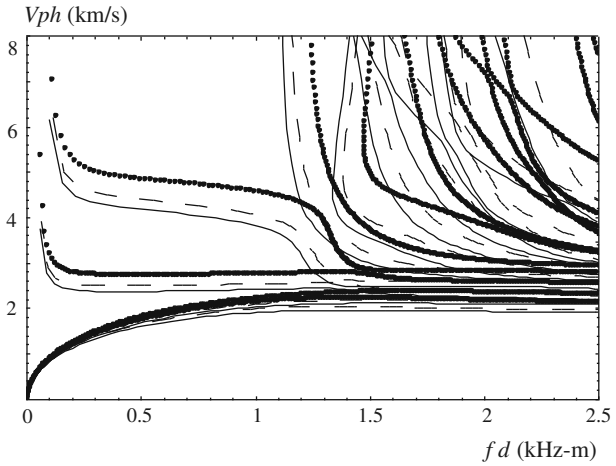

Fig. 5 Phase velocity dispersion curves for r-polarized and linearly a-FGPM square rings with $\eta = 10$ (*solid lines* linearly FGPM ring, *dashed lines* quadratically FGPM ring, *dotted lines* cubically FGPM ring)

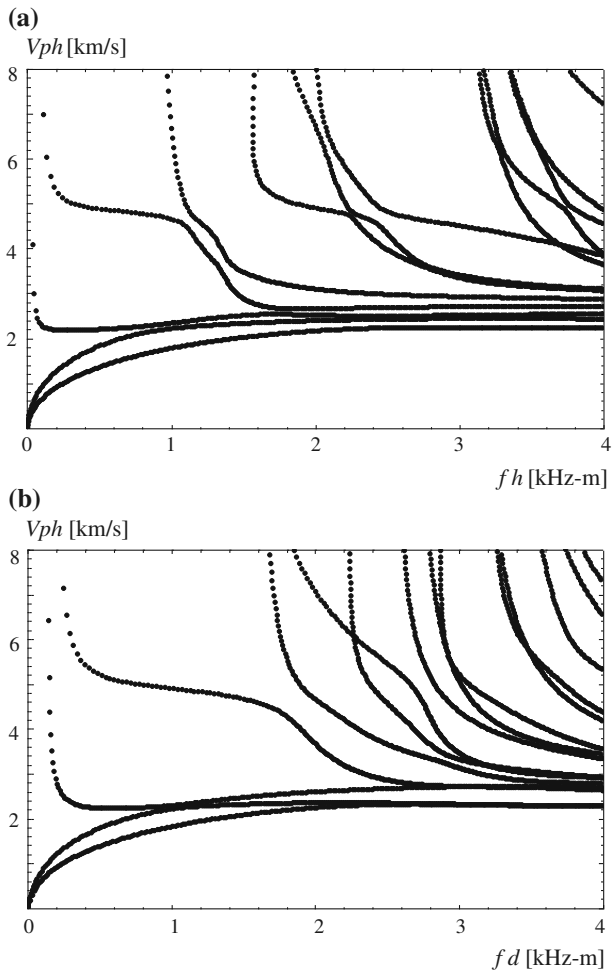

Fig. 6 Phase velocity dispersion curves for r-polarized linearly FGPM rectangular rings with $\eta = 10$: **a** linearly a-FGPM ring with $d/h = 2$, **b** linearly r-FGPM ring with $d/h = 0.5$

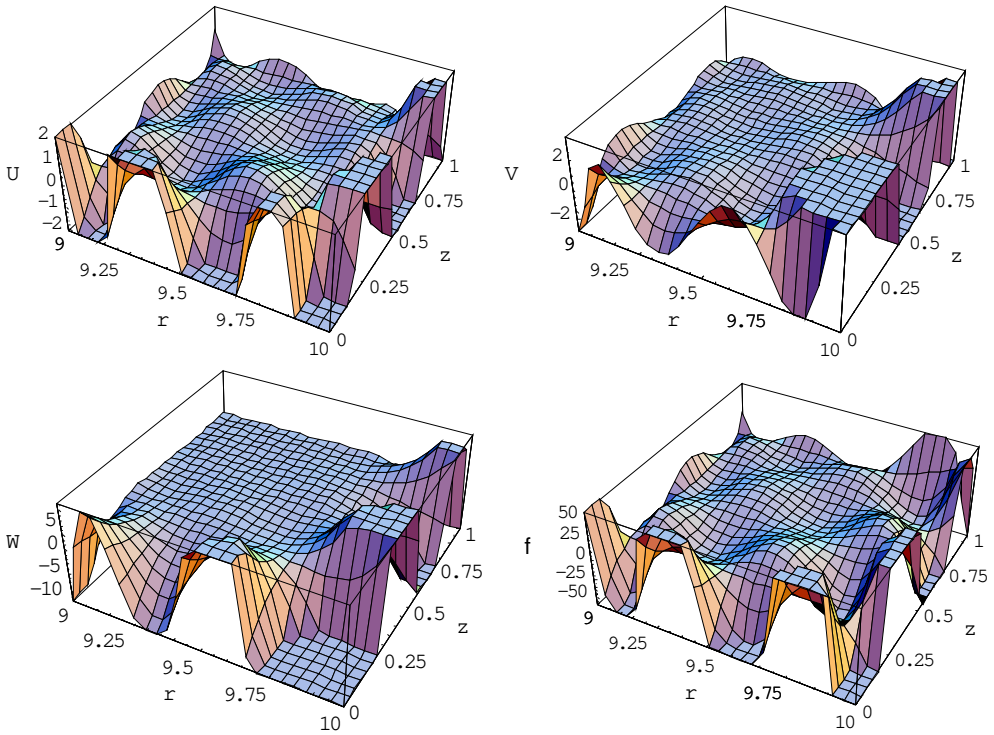

Fig. 7 Mechanical displacement and electric potential profiles of the first wave mode for the r-polarized and linearly a-FGPM square ring with $\eta = 10$ at $kd = 90.1$

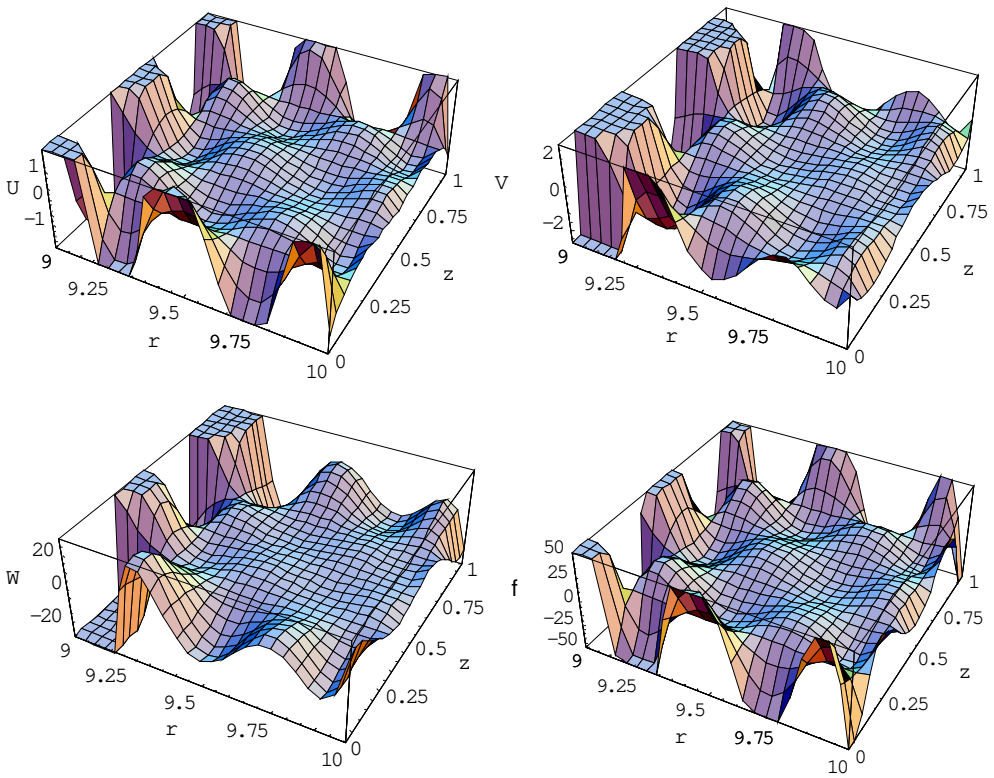

Fig. 8 Mechanical displacement and electric potential profiles of the first wave mode for the r-polarized and linearly r-FGPM square ring with $\eta = 10$ at $kd = 90.1$

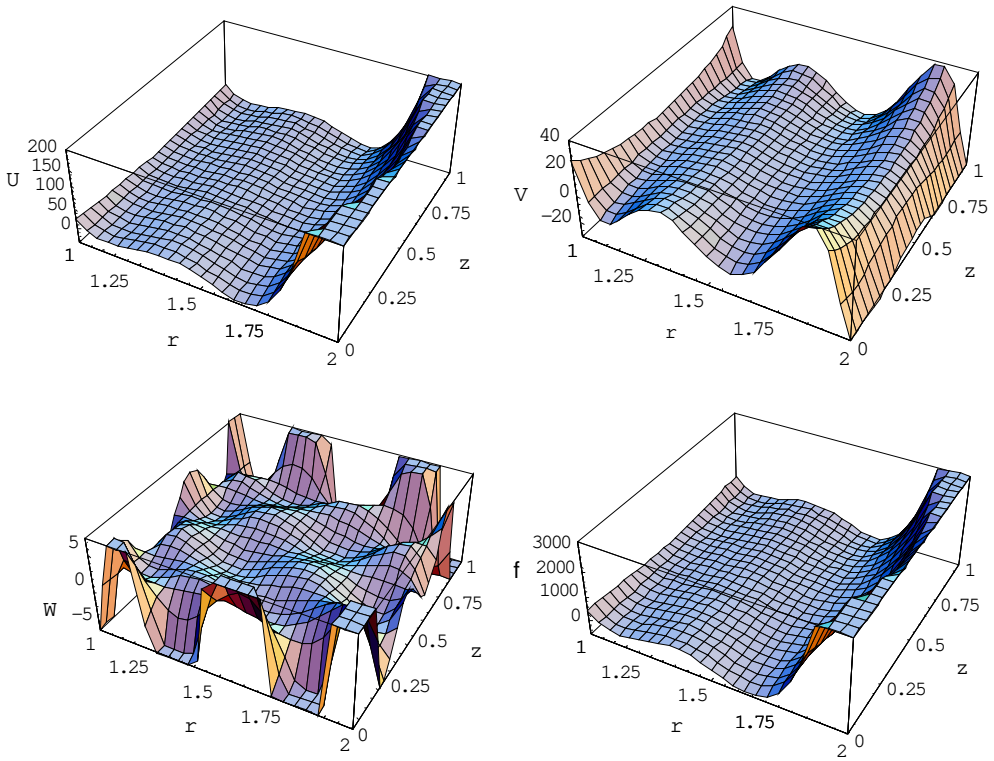

Fig. 9 Mechanical displacement and electric potential profiles of the first wave mode for the r-polarized and linearly r-FGPM square ring with $\eta = 2$ at $kd = 90.1$

elastic constants of a radially polarized (rp) and axially polarized (ap) r-FGPM ring are taken the same in order to make appropriate comparisons.

Firstly, three linearly ($V_1(r) = [(r-a)\,/\,(b-a)]$ for r-FGPM rings and $V_1(z) = z/h$ for a-FGPM rings) FGPM square rings with $\eta = 10$ are considered. They are: (a) r-polarized r-FGPM ring, (b) a-polarized r-FGPM ring, (c) r-polarized a-FGPM ring. Their phase velocity dispersion curves are shown in Fig. 3a, and the phase velocity dispersion curves for rings of their correspondingly small radius to thickness ratio ($\eta = 2$) are shown in Fig. 3b. Rings (a) and (b) just have different polarization directions, and rings (a) and (c) just have different gradient directions. When radius to thickness ratio is large, the polarization direction has considerable influences on the dispersion curves, but the gradient direction just has weak influences. When radius to thickness ratio is small, both the polarization direction and the gradient direction have significant influences. In fact, the material volume fractions of the linearly r-FGPM ring and the linearly a-FGPM ring are different. In the linearly r-FGPM ring, the volume fraction of PZT-4 is smaller than that of BSN. But in a linearly a-FGPM ring, the volume fraction of PZT-4 equals that of BSN. And the wave speed of PZT-4 is lower than that of BSN. So, the phase velocities of a linearly a-FGPM ring are lower than those of a linearly r-FGPM ring. Furthermore, as the radius to thickness ratio decreases, the volume fraction of PZT-4 in a linearly r-FGPM ring becomes smaller, but the volume fraction of PZT-4 in a linearly a-FGPM ring does not change. So, as η decreases, the difference of the phase velocity between linearly a-FGPM ring and linearly r-FGPM ring becomes larger.

Next, the influence of radius to thickness ratio is discussed. The material volume fractions in a-FGPM rings do not change as the radius to thickness ratio changes. So, the r-polarized and linearly a-FGPM square rings with $\eta = 10$, 5, 3 and 2 are calculated, respectively. Their phase velocity dispersion curves are shown in Fig. 4. It can be seen that as the radius to thickness ratio decreases, the dispersion becomes more serious and the phase velocity becomes higher.

Then, three r-polarized and a-FGPM square rings with $\eta = 10$ are considered. Their gradient shapes are $V_1(z) = (z/h)^n$, $n = 1, 2, 3$, i.e, linear, quadratic and cubical. The corresponding dispersion curves are shown in Fig. 5. Figure 5 illustrates that the gradient shapes can significantly influence the dispersion curves. As n increases, the volume fraction of PZT-4 increases, which results in the wave velocity becoming lower.

The above structures all have square cross-sections. Next, two r-polarized (rp) linearly FGPM rectangular rings with $\eta = 10$ are considered. They are on a-FGPM ring with $d/h = 2$ and on r-FGPM ring with $d/h = 0.5$. The corresponding phase velocity dispersion curves are shown in Fig. 6. We can see that the thickness to height ratio may also influence the dispersion curves significantly.

3.3 Mechanical displacement and electric potential profiles for FGPM rectangular rings

This section discusses the guided wave characteristics by analyzing the mechanical displacement and electric potential profiles. Firstly, the mechanical displacement and the electric potential profiles at $kh = 90.1$ for the first wave mode of the ring (b) are illustrated in Fig. 7. It can be seen that the mechanical displacements and the electric potential mainly distribute near the bottom and outside edges. Then, Fig. 8 shows the case of the ring (a). It can be seen that the mechanical displacements and the electric potential are mainly concentrated near the edges except on the outside edge, and the mechanical displacements mostly distribute near the inner edge. According to a comprehensive analysis of the two figures, we can conclude that the high-frequency guided waves mainly distribute on the side with more PZT-4 phase because of the fact that the bulk wave speed of the PZT-4 is lower than that of the BSN. Simultaneously high-frequency guided waves approach four edges (mostly outside edges). Finally, the result for the case of a small radius to thickness ratio $\eta = 2$ of the ring (a) is illustrated in Fig. 9. It can be seen that the mechanical displacements and the electric potential do not distribute near the side with more PZT-4 phase but mostly near the outside edge. This is due to the fact that for rings with small radius to thickness ratios the mechanical displacements and the electric potential approach outside edges.

4 Conclusions

This paper presents a double orthogonal polynomial approach to analyzing wave propagation in 2-D FGPM rectangular rings. Numerical comparison of the obtained dispersion curves with reference solutions shows that the present extended orthogonal polynomial method is appropriate to solve the guided wave propagation problems in 2-D FGPM structures. The dispersion curves, the displacement and electric potential distributions of various FGPM rectangular rings are presented and discussed. According to the present numerical results, we can conclude that the material gradient shapes, the width to height ratio, the gradient direction, the radius to thickness ratio and the polarization direction may all influence the guided wave characteristics significantly. High-frequency guided waves propagate predominantly in the side with more material phase having lower wave speed, and simultaneously, they approach the outside edges, especially for rings with small radius to thickness ratios.

Acknowledgments This work was supported by the National Natural Science Foundation of China (No. 11272115), the Outstanding Youth Science Foundation of Henan Polytechnic University (No. J2013-08) and Henan Province (No. 144100510016). Jiangong Yu also gratefully acknowledges the support by the Alexander von Humboldt-Foundation (AvH) to conduct his research works at the Chair of Structural Mechanics, Faculty of Science and Technology, University of Siegen, Germany.

References

1. Wu, C.C.M., Kahn, M., Moy, W.: Piezoelectric ceramics with functional gradients: a new application in material design. J. Am. Ceram. Soc. **79**, 809–812 (1996)
2. Takagi, K., Li, J.F., Yokoyama, S., Watanabe, R.: Fabrication and evaluation of PZT/Pt piezoelectric composites and functionally graded actuators. J. Eur. Ceram. Soc. **23**, 1577–1583 (2003)
3. Zhu, X., Zhu, J., Zhou, S., Li, Q., Liu, Z.: Microstructures of the monomorph piezoelectric ceramic actuators with functional gradients. Sensors Actuators A Phys. **74**, 198–202 (1999)
4. Li, X., Vartuli, J.S., Milius, D.L., Aksay, I.A., Shih, W.Y., Shih, W.H.: Electromechanical properties of a ceramic d31-gradient flextensional actuator. J. Eur. Ceram. Soc. **84**, 996–1003 (2001)
5. Li, J.F., Takagi, K., Ono, M., Pan, W., Watanabe, R.: Fabrication and evaluation of porous ceramics and porosity-graded piezoelectric actuators. J. Eur. Ceram. Soc. **86**, 1094–1098 (2003)
6. Chen, Y.H., Ma, J., Li, T.: A functional gradient ceramic monomorph actuator fabricated using electrophoretic deposition. Ceram. Int. **30**, 683–687 (2004)
7. Qui, J., Tani, J., Ueno, T., Morita, T., Takahashi, H., Du, H.: Fabrication and high durability of functionally graded piezoelectric bending actuators. Smart Mater. Struct. **12**, 115–121 (2003)
8. Jin, D., Meng, Z.: Functionally graded PZT/ZnO piezoelectric composites. J. Mater. Sci. Lett. **22**, 971–974 (2003)

9. Liu, G.R., Tani, J.: Characteristics of wave propagation in functionally gradient piezoelectric material plates and its response analysis: Part 1: Theory, Part 2: Calculation results. Trans. Jpn. Soc. Mech. Eng. Jpn. **57(A)**, 2122–2133 (1991)
10. Han, X., Liu, G.R.: Elastic waves in a functionally graded piezoelectric cylinder. Smart Mater. Struct. **12**, 962–971 (2003)
11. Liu, G.R., Dai, K.Y., Han, X., Ohyoshi, T.: Dispersion of waves and characteristic wave surfaces in functionally graded piezoelectric plates. J. Sound Vib. **268**, 131–147 (2003)
12. Chakraborty, A., Roy Mahapatra, D., Gopalakrishnan, S.: Finite element simulation of BAW propagation in inhomogeneous plate due to piezoelectric actuation. In: Lecture Notes in Computer Science, pp. 715–724 (2003)
13. Chakraborty, A., Gopalakrishnan, S., Kausel, E.: Wave propagation analysis in inhomogeneous piezo-composite layer by the thin-layer method. Int. J. Numer. Methods Eng. **64**, 567–598 (2005)
14. Roy Mahapatra, D., Singhal, A., Gopalakrishnan, S.: Lamb wave characteristics of thickness-graded piezoelectric IDT. Ultrasonics **43**, 736–746 (2005)
15. Hasheminejad, S.M., Alaei-Varnosfaderani, M.: Vibroacoustic response and active control of a fluid-filled functionally graded piezoelectric material composite cylinder. J. Intell. Mater. Syst. Struct. **23**, 775–790 (2012)
16. Li, X.Y., Wang, Z.K., Huang, S.H.: Love waves in functionally graded piezoelectric materials. Int. J. Solids Struct. **41**, 7309–7328 (2004)
17. Liu, J., Wang, Z.K.: The propagation behavior of Love waves in a functionally graded layered piezoelectric structure. Smart Mater. Struct. **14**, 137–146 (2005)
18. Gao, L.M., Wang, J., Zhong, Zh., Du, J.K.: An analysis of surface acoustic wave propagation in functionally graded plates with homotopy analysis method. Acta Mech. **208**, 249–258 (2009)
19. Lefebvre, J.E., Zhang, V., Gazalet, J. et al.: Acoustic wave propagation in continuous functionally graded plates, an extension of the Legendre polynomial approach. IEEE Trans. Ultrason. Ferroelectr. Freq. Control **48**, 1332 (2001)
20. Yu, J.G., Wu, B., Chen, G.Q.: Wave characteristics in functionally graded piezoelectric hollow cylinders. Arch. Appl. Mech. **79**, 807–824 (2009)
21. Du, J.K., Jin, X.Y., Wang, J., Xian, K.: Love wave propagation in functionally graded piezoelectric material layer. Ultrasonics **46**, 13–22 (2007)
22. Datta, S., Hunsinger, B.J.: Analysis of surface waves using orthogonal functions. J. Appl. Phys **49**, 475–479 (1978)
23. Yu, J.G., Wu, B., Huo, H.L., He, C.F.: Characteristics of guided waves in anisotropic spherical curved plates. Wave Motion **44**, 271–281 (2007)
24. Wu, B., Yu, J.G., He, C.F.: Wave propagation in non-homogeneous magneto-electro-elastic plates. J. Sound Vib. **317**, 250–264 (2008)
25. Yu, J.G., Wu, B., He, C.F.: Guided thermoelastic waves in functionally graded plates with two relaxation times. Int. J. Eng. Sci. **48**, 1709–1720 (2010)
26. Yu, J.G.: Viscoelastic shear horizontal wave in graded and layered plates. Int. J. Solids Struct. **48**, 2361–2372 (2011)
27. Hayashi, T., Song, W.-J., Rose, J. L.: Guided wave dispersion curves for a bar with an arbitrary cross-section, a rod and rail example. Ultrasonics **41**, 175–183 (2003)